Structure
Article

An IgG-like Domain in the Minor Pilin GBS52 of *Streptococcus agalactiae* Mediates Lung Epithelial Cell Adhesion

Vengadesan Krishnan,[1,3] Andrew H. Gaspar,[2,3] Naiqing Ye,[2] Anjali Mandlik,[2] Hung Ton-That,[2,*] and Sthanam V.L. Narayana[1,*]
[1] School of Optometry and Center for Biophysical Sciences and Engineering, University of Alabama at Birmingham, Birmingham, AL 35294, USA
[2] Department of Molecular, Microbial, and Structural Biology, University of Connecticut Health Center, Farmington, CT 06030, USA
[3] These authors contributed equally to this work.
*Correspondence: ton-that@uchc.edu (H.T.-T.), narayana@uab.edu (S.V.L.N.)
DOI 10.1016/j.str.2007.06.015

SUMMARY

Streptococcus agalactiae **is the leading cause of neonatal pneumonia, sepsis, and meningitis. The pathogen assembles heterotrimeric pilus structures on its surface; however, their function in pathogenesis is poorly understood. We report here the crystal structure of the pilin GBS52, which reveals two IgG-like fold domains, N1 and N2. Each domain is comprised of seven antiparallel β strands, an arrangement similar to the fold observed in the *Staphylococcus aureus* adhesin Cna. Consistent with its role as an adhesin, deletion of *gbs52* gene significantly reduces bacterial adherence to pulmonary epithelial cells. Moreover, latex beads linked to the GBS52 protein adhere to pulmonary but not to many other epithelial cells; binding to the former is specifically inhibited by antibodies against GBS52. Nonetheless, substantial binding is only observed with N2 domain-conjugated beads. This study presents the structure of a Gram-positive pilin that utilizes a distinct IgG fold variant to mediate pathogen adherence to a specific tissue.**

INTRODUCTION

The Gram-positive bacterial pathogen *Streptococcus agalactiae* (group B *streptococcus*; GBS) is the leading cause of neonatal pneumonia, sepsis, and meningitis leading to significant morbidity and mortality in the United States and Europe (Baker and Edward, 2001). Streptococcal pathogenesis begins with bacterial adherence to epithelial host tissues, followed by invasion and host tissue damage, avoidance of immunologic clearance, and activation of inflammatory responses (Doran and Nizet, 2004). Several GBS virulence factors that contribute to these steps have been characterized (Spellerberg, 2000); however, colonization factors that are critical for bacterial adherence are largely unknown.

The cell wall of Gram-positive bacteria harbors key molecules that allow the pathogen to interact with specific host cells. Typically, these pathogens use a variety of surface-displayed proteins and proteinaceous filaments, such as pili or fimbriae that are covalently anchored to the cell wall for interactions with the host, leading to the establishment of commensal or pathogenic relationships. Extensive structural studies of the surface proteins have provided insights into their assembly and adhesive properties (Marraffini et al., 2006; Patti et al., 1994; Ponnuraj et al., 2003; Symersky et al., 1997). In contrast, although pili have been identified in several Gram-positive pathogens, their mechanisms of assembly and function are just beginning to be elucidated (Scott and Zahner, 2006; Telford et al., 2006; Ton-That and Schneewind, 2004).

The best-understood system of Gram-positive pilus assembly is found in *Corynebacterium diphtheriae*, the causative agent of diphtheria that assembles three distinct pilus structures on its surface, designated as SpaA-, SpaD-, and SpaH-type pili (Gaspar and Ton-That, 2006; Swierczynski and Ton-That, 2006; Ton-That and Schneewind, 2003). The prototype SpaA-type pilus (sortase-mediated *p*ilus *a*ssembly) is composed of SpaA forming the pilus shaft, SpaB decorating the shaft, and SpaC largely located at the tip region (Ton-That and Schneewind, 2003). Recently, it has been shown that the minor pilins SpaB and SpaC are not only components of pili but are also displayed throughout the bacterial surface through covalent anchoring to the cell wall (Mandlik et al., 2007). Similar to the surface protein MSCRAMMs (*m*icrobial *s*urface *c*omponent *r*ecognizing *a*dhesive *m*atrix *m*olecules), these pilin subunits carry an N-terminal signal peptide and a C-terminal sorting signal consisting of an LPXTG sorting motif, followed by a hydrophobic domain and a positively charged tail (Fischetti et al., 1990). In addition to the C-terminal sorting signal, SpaA contains a conserved element called the pilin motif, which is absolutely required for pilus formation (Ton-That et al., 2004). Whereas *spaB* and *spaC* are dispensable, deletion of *spaA* abrogates the formation of pilus fibers (Ton-That et al., 2004). The assembly of SpaABC pilus requires a specific sortase, SrtA, encoded within the pilus gene cluster (Ton-That and

Schneewind, 2003). According to the current working model (Ton-That and Schneewind, 2004), sortase SrtA cleaves the LPXTG motif of SpaA between threonine and glycine and peptide links the nascent C-terminal threonine to a conserved lysine side chain within the pilin motif of another SpaA to generate covalent crosslinks between pilin subunits. The crosslinked pilin polymers are then covalently joined to the peptidoglycan crossbridge of the bacterial cell wall. SpaC is linked at the tip region, presumably by a similar mechanism involving the SpaC sorting signal and the SpaA pilin motif, whereas SpaB incorporation into the pilus structure requires a conserved glutamate of the SpaA E box by an unknown linkage (Ton-That et al., 2004).

The aforementioned mechanism of pilus assembly appears to be conserved in many Gram-positive bacteria, including *Actinomyces*, *C. diphtheriae*, group A streptococci, *Streptococcus pneumoniae*, *Enterococcus faecalis*, and *S. agalactiae* (Barocchi et al., 2006; Mishra et al., 2007; Mora et al., 2005; Nallapareddy et al., 2006; Ton-That et al., 2004). Genomic analysis of GBS strains 2603V/R, NEM316, and A909 revealed the presence of two similar pilus islands (PIs) that encode a number of LPXTG motif-bearing proteins and sortases (Dramsi et al., 2006; Rosini et al., 2006). Electron microscopy and biochemical studies have shown that the PI-1 in strain 2603V/R encodes a pilus structure composed of a major subunit GBS80 and two minor pilins (or auxiliary proteins) GBS52 and GBS104 (Rosini et al., 2006) (see Figure 1A). Similar to corynebacterial SpaA, GBS80 forms the pilus shaft into which GBS52 and GBS104 are incorporated (Rosini et al., 2006). Based on their structural organization, GBS52 and GBS104 may be counterparts of corynebacterial SpaB and SpaC. It is possible that GBS104 and GBS52 are covalently linked to the pilus structures involving the pilin motif and the E box of the major subunit GBS80.

Paralogous to GBS52 is the minor pilin GBS150 (32% identity) of the PI-2 in strain 2603V/R (Rosini et al., 2006). GBS150 pilin is polymerized into high-molecular weight structures as detected by immunoblotting, and this polymerization is dependent on the major subunit GBS67 and a pilin-specific sortase, SAG1406 (Rosini et al., 2006). In strain NEM316, the minor pilin called GBS1474 is an ortholog of GBS52 (Dramsi et al., 2006; Rosini et al., 2006). Interestingly, by immunoelectron microscopy, GBS1474 labels were observed mostly at the base of the pilus and at random along the pilus shaft (Dramsi et al., 2006). The deletion of *gbs1474* does not abolish pilus assembly, as is true for *gbs52* and *gbs150* deletions (Dramsi et al., 2006; Rosini et al., 2006). Intriguingly, adherence to lung and cervical epithelial cells is significantly reduced in the *gbs1474* mutant but not in the *gbs1477* deletion mutant, which is devoid of the pilus shaft (Dramsi et al., 2006). This result suggests that the minor pilin GBS1474 plays a role in adhesion. The same conclusion was recently reached for corynebacteria: the minor pilins SpaB and SpaC are utilized by the pathogen to target human pharyngeal epithelial cells (Mandlik et al., 2007). Although these studies emphasize the function of minor pilins in host-bacterial adhesion, the specific role of GBS52 in streptococcal adherence has not been addressed to date.

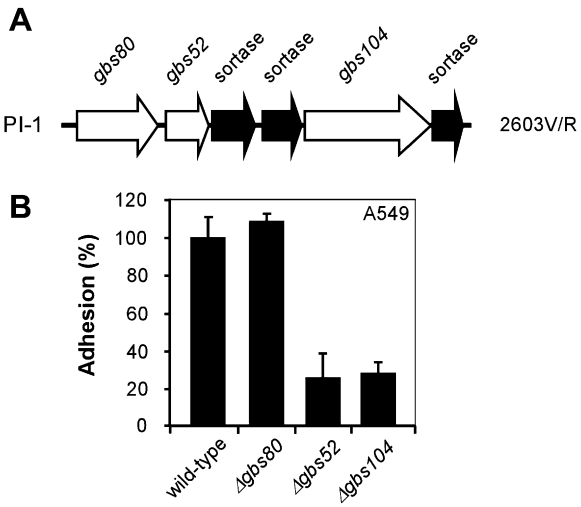

Figure 1. Minor Pilins Are Required for Streptococcal Adherence

(A) Graphic representation of GBS pilus island 1 (PI-1) from strain 2603V/R with three sortase genes, along with three sortase-mediated pilus assembly genes (*gbs80*, *gbs52*, and *gbs104*).

(B) Requirement of GBS52 for streptococcal adhesion to lung epithelial cells. Confluent monolayers of lung epithelial cells (A549) were infected with the wild-type and its isogenic deletion mutants, and adherent bacteria were then enumerated. Data are presented as percentage of adhesion relative to that of wild-type. The results are presented as averages (with standard deviations; ±SD) from at least three independent experiments performed in quadruplicate.

We report here the crystal structure of GBS52 and show that IgG-like domains of this minor pilin mediate specific adherence to host tissues. Our studies provide structural insights for the first time, to our knowledge, into the assembly and function of a Gram-positive bacterial pilin.

RESULTS AND DISCUSSION

Requirement of *gbs52* for *Streptococcus agalactiae* Adherence to Human Pulmonary Epithelial Cells

As noted above, the PI-1 in strain 2603V/R (Figure 1A) encodes a distinct pilus structure that is composed of a major subunit, GBS80, and two minor pilins, GBS52 and GBS104 (Rosini et al., 2006). To determine whether the PI-1 pili are involved in GBS adherence to host tissues, we generated nonpolar in-frame deletion mutants of GBS that lack individual pilus components. We then examined the relative association of streptococcal variants with lung epithelial cells (A549) in culture. These cells were grown in multiwell culture plates in RPMI media to confluence and infected with streptococci. The infected cells were washed to remove the unbound bacteria, detached from wells, and plated on agar plates to enumerate bacteria absorbed by the epithelial cells (see Experimental Procedures). The binding of GBS variants to lung epithelial cells was then compared to that of the wild-type strain, which was set to 100% (Figure 1B, first column). Importantly, deletion of

gbs80, which was reported to abrogate the assembly of the PI-1 pili (Rosini et al., 2006), did not affect bacterial adherence to lung epithelial cells (Figure 1B, second column). Thus, the PI-1-encoded pilus fibers are not essential for streptococcal adherence to host cells. Interestingly, the deletion of either *gbs52* or *gbs104* strikingly reduced bacterial adherence to pulmonary cells (2.5-fold reduction; Figure 1B, last two columns). However, antibodies against GBS52 did not block adherence to lung cells by the wild-type bacteria (data not shown). These results demonstrate that the GBS52 and GBS104 pilins act independently to promote the effective binding of the pathogen to pulmonary cells.

Crystal Structure of the GBS52 Recombinant Protein

Toward understanding the nature and architecture of the GBS pili, we determined the three-dimensional structure of the GBS52 pilin using X-ray crystallography. The recombinant protein GBS52 (Figure 2A) was expressed in *Escherichia coli*, purified, and crystallized (see Experimental Procedures). The crystal structure of GBS52 is determined by multiple isomorphous replacement methods (Tables 1 and 2) and refined to an R factor of 19.7 and R_{free} of 23.1% (Table 3). The overall structure of GBS52 is shown in cartoon form in Figure 2B. Overall, the GBS52 structure displays a two-domain architecture, in which each of the domains is made of a common immunoglobulin-like (IgG-like) β sandwich fold, with some variations in the order of β strand arrangement (see below).

The cloned GBS52 protein consists of 237 amino acids (His31–Arg267) (Figure 2A) with an N-terminal His_6 tag. The His_6 tag residues were not seen in electron density maps. The crystal structure of GBS52 revealed that it is made of two β barrel domains (N1 and N2) connected by a short linker. The overall structure resembles a bent rod, with approximate overall dimensions of 30 × 45 × 85 Å (Figure 2B). The core of each domain is made of seven antiparallel β strands grouped into two β sheets: one sheet of four β strands (CBEF) and the other with three β strands (DAG). The N1 domain, made of seven shorter β strands, is stocky looking and decorated with two long linker loops that cover both sides. A hook-shaped "AB loop," carrying a single-turn 3_{10}-helical segment and stabilized by two short β strands, is inserted between the A and B β strands. Another "BC loop," inserted between the B and C β strands, displays two α-helical segments (Figure 2B). By comparison, the rod-like N2 domain is tall and lean and displays an extended proline-rich, 12 residue C-terminal tail (Figure 2B). The AB loop of the N2 domain is quite short, whereas its BC loop, displaying a rather unique convoluted shape and carrying two short antiparallel β strands, has electron density only for its main-chain atoms in $2F_o - F_c$ maps. A short β strand, present in both the N1 and N2 domains, stabilizes their EF loops by interacting with respective E and G strands.

Comparison of GBS52 N1 and N2 Domains

Only 13% primary sequence identity is found between the two IgG-like domains of GBS52. The N1 domain consists

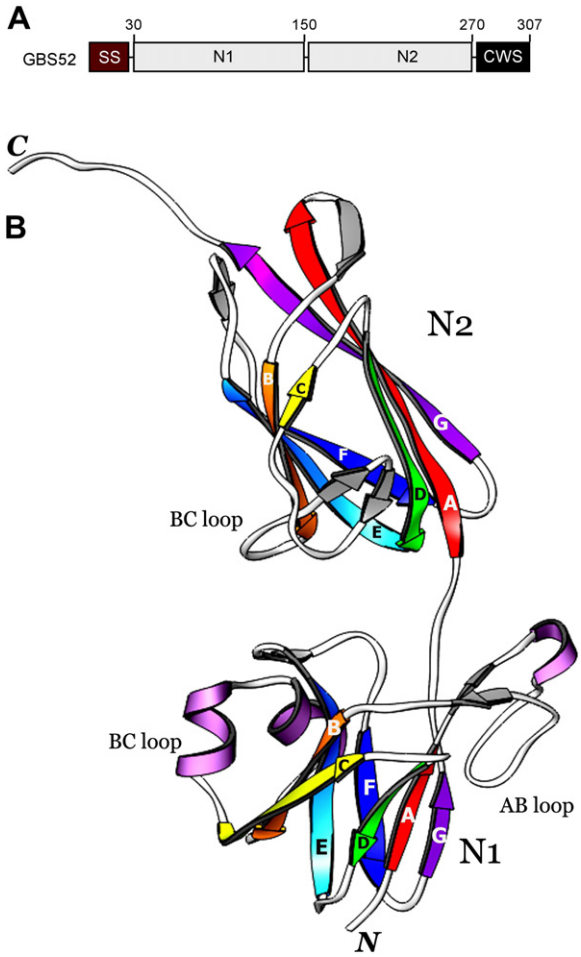

Figure 2. The Structure of the Minor Pilin GBS52

(A) Schematic domain organization of GBS52. GBS52 contains an N-terminal signal sequence (SS), followed by the 120 residue N1 domain, 116 residue N2 domain, and a C-terminal cell wall sorting signal (CWS).

(B) Ribbon diagram of the overall crystal structure of GBS52. The two domains N1 and N2 are placed vertically to the plane of the paper. The strands of both N1 and N2 domains are assigned with rainbow colors (from red [A] to violet [G]) for comparison with other topologically related domains.

of 120 residues (His31–Ile150) with approximate overall dimensions of 23 × 33 × 40 Å, whereas the N2 domain consists of 116 residues (Ser152–Arg267) with approximate overall dimensions of 24 × 24 × 46 Å. The two domains can be superimposed with a root-mean-square (rms) deviation of 1.3 Å for 65 common Cα atoms (Figure 3A). Although their topology is identical, there are subtle structural differences between the two domain structures. The N2 domain has an extended C-terminal tail; with a longer G strand, its AB loop is much shorter than in N1. The significant difference is in the BC loop size and shape, where a slight structural displacement is seen between the EF loops when superposed, as their tips are seen pointing away from each other. Hydrophobic cores are built by a number of hydrophobic residues, both in the

Table 1. GBS52 Native and Heavy-Atom Derivative Crystallographic Data

Parameter	Native	$Hg(CH_3COO)_2$	K_2PtCl_4	$Ag(NO)_3$
a (Å)	41.48	41.53	41.56	41.66
b (Å)	52.22	52.23	52.05	52.16
c (Å)	61.01	60.89	60.84	61.13
β (°)	101.79	101.9	101.65	101.92
Resolution (Å)	26.8–1.8 (1.86–1.8)	23.9–2.5 (2.59–2.5)	21.9–2.5 (2.59–2.5)	20.0–2.5 (2.59–2.5)
R_{merge} (%)	0.04 (0.15)	0.07 (0.09)	0.04 (0.08)	0.04 (0.06)
Unique reflections	23,655	8,731	8,684	8,089
Redundancy	3.01 (2.33)	3.70 (3.65)	3.64 (3.53)	2.98 (2.84)
Completeness (%)	99.4 (97.3)	97.4 (95.8)	97.2 (94.6)	89.9 (91.4)
I/σI	14.3 (4.6)	13.6 (10.4)	21.6 (12.3)	21.8 (15.1)

Values in parentheses are for the last resolution shell.

N1 (Leu33, Leu67, Phe98, Ala108, Phe110, Leu113, Val132, Phe135, Val137, Leu139, Ile145, Pro147, Ile149) and N2 (Leu156, Leu158, Val174, Phe176, Leu178, Ile212, Ile214, Leu217, Leu224, Val242, Ile244, Val250, Val252, Ile254) domains.

The proline-rich hydrophobic C terminus of GBS52 is in an extended conformation. Interestingly, it is stabilized and sequestered by hydrophobic interactions from neighboring symmetry-related GBS52 molecules. One side (Lys258, Pro260, Pro262, Lys263, Val264, Pro265, Ser266) of this tail is stabilized by the N1 domain of a symmetry-related neighboring molecule, where the stabilizing contacts are mainly from the AB loop (Lys91), C strand (Gln95, Gln96, Val97, Phe98, Glu99), and DE loop (Asn111, Gln112) of the neighbor. The other side (Val259, Thr261, Pro262, Lys263, Val264, Pro265, Ser266, Arg267) is stabilized by the N1 and N2 domain interface of another symmetry-related molecule, where the interactions come from part of the BC (His194, Gln196, Ile198), AB (Glu39), and FH (Ser247, Lys248, Thr249) loops and strand D (Gly216, Ile218) of its N2 domain. These interactions are crystallographic artifacts; however, it is possible that the hydrophobic environment observed around the C-terminal extension is a reflection of its actual surroundings, possibly contributed by the neighboring, either GBS52 or GBS80, molecules during pilus assembly.

Domain Interface

A tryptophan residue (Trp151) present in the short linker between the N1 and N2 domains seems to play a crucial role in domain arrangement, by creating an interdomain hydrophobic core. The buried surface area for the interface between the N1 and N2 domains is 943 $Å^2$. The interface is contributed by a total of 23 residues from both domains, half of which are charged amino acids. The residues of the two domains make 13 contacts measuring less than 4 Å, including two salt bridges (Asp42-Lys246, Glu127-Arg184).

Table 2. Heavy-Atom Derivative Statistics for GBS52[a]

Heavy-Atom Compound	Number of Sites	R_{iso}	$R_{centric}$	RMS(FH)/RMS(E)
$Hg(CH_3COO)_2$	2	0.28	0.60	1.31
K_2PtCl_4	2	0.23	0.61	0.92
$Ag(NO)_3$	2	0.22	0.76	0.76

[a] Overall figures of merit after density modification 0.61.

Three-Dimensional Alignment with Dali

In our efforts to identify structures of similar topology available in the Protein Data Bank (PDB), the Dali program (Dietmann et al., 2001) generated the best fit with the first β sandwich domain (SD1) of Ferovidolysin (PDB ID code 1R6V), a bacterial enzyme involved in keratin degradation, followed by the C-terminal subdomain (CTSD) of Carboxypeptidase D domain II (PDB ID code 1QMU), an avian prohormone/propeptide processing enzyme (Gomis-Ruth et al., 1999; Kim et al., 2004). The N2 domain comparison with Dali gave almost similar hits, but the CTSD becomes the top best fit followed by the SD1 domain. The SD1 and CTSD have exactly the same topology and composition

Table 3. Refinement Statistics for GBS52 Structure

Parameter	GBS52
Resolution range	30–1.8
R factor/R_{free} (%)	19.7/23.1
Average B value ($Å^2$)	18.7
Rms deviation for bonds (Å)	0.017
Rms deviation for angles (°)	1.561
Number of protein atoms	1,871
Number of water molecules	223
Unique reflections	23,655
Ramachandran plot (allowed/disallowed)	100.0/0.0

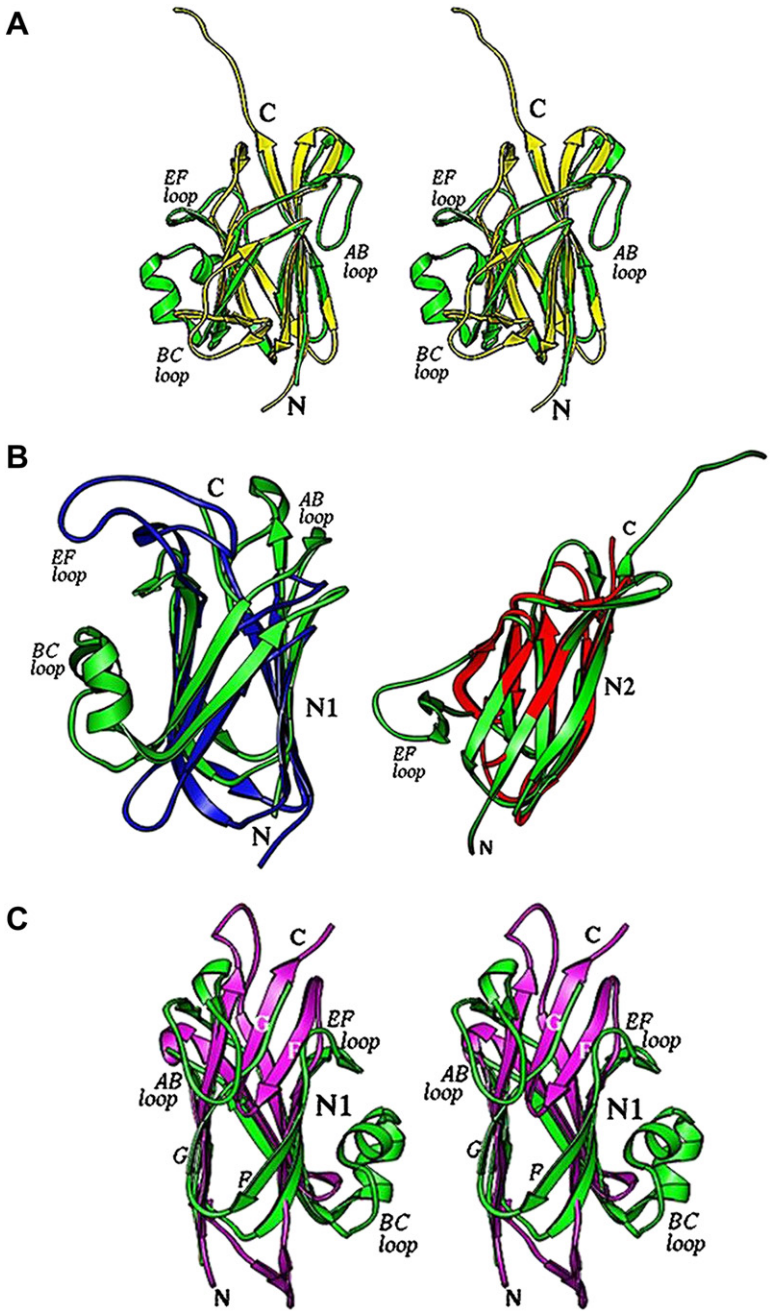

Figure 3. GBS52 Domain Comparison

(A) A stereo-view ribbon diagram of the superposition of the N1 domain (green) and the N2 domain (yellow) of GBS52. The variable regions are labeled (AB, BC, and EF loops and C-terminal tail).

(B) Comparison of GBS52 domains with other best topologically and structurally related domains in the Protein Data Bank as found by the Dali server (Dietmann et al., 2001). Left: superposition of the N1 domain (green) of GBS52 and first β sandwich domain (SD1) of Ferovidolysin (in blue; PDB ID code 1R6V). Right: superposition of the N2 domain (green) of GBS52 and C-terminal subdomain of Carboxypeptidase D domain II (in red; PDB ID code 1QMU).

(C) A stereo view of structural comparison of the N1 domain of GBS52 (green) with the Cna B region subdomain D1 (magenta). Main differences are seen in the loops and strand F position.

of three (DAG)- and four (CBEF)-stranded β sheet arrangement, but the sequence identity between them is less than 17%. The structural superposition of the N1 domain of GBS52 with SD1 resulted in an rms deviation of 1.5 Å for 42 common Cα atoms. Similarly, the structural superposition of the N2 domain of GBS52 with CTSD resulted in an rms deviation of 1.5 Å for 68 common Cα atoms (Figure 3B).

Topology Comparison of GBS52 N1 and N2 Domains with the IgG Constant Domain

The SD1 and CTSD structures were described as simple IgG-like domains (Gomis-Ruth et al., 1999; Kim et al., 2004). However, we noticed that the order of β strand arrangement in these structures is unlike that seen in IgG-like domains and observed the topology of CD1 and CTSD structures closer to the arrangement seen in the GBS52 N1 and N2 domains. To understand this unique disposition of β strands, we compared the N1 and N2 domains of GBS52 to the IgG constant domain (PDB ID code 1DBB). The IgG constant domain generally has a four-stranded antiparallel β sheet ABED on one side of the barrel and a three-stranded antiparallel β sheet CFG on the other side (see Figure 4A). The structural superposition of the GBS52 N1 domain with the IgG constant domain resulted in an rms deviation of 1.9 Å for 23 commons Cα

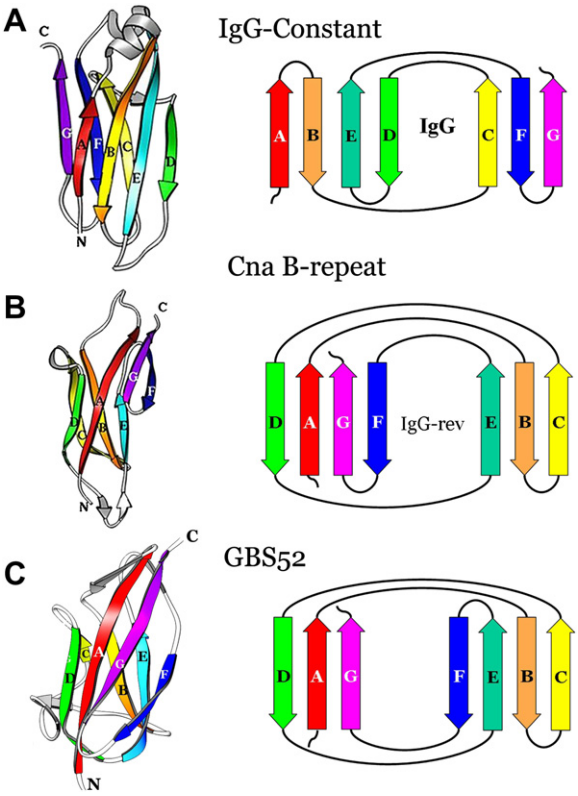

Figure 4. Topology Comparison

Arrows represent the β strands colored similarly to the Figure 2 representation. Shown are the IgG constant domain (A), the D1 domain of the B1 region of *S. aureus* collagen-binding protein Cna (B), and the N1 domain of GBS52 (C). The D1 resembles the IgG-like structure with a four- and three-β-stranded barrel, but exhibits a novel IgG-rev fold. The β sandwich structures are compared as follows: (IgG/D1) A/F, D/C, C/D, B/E, E/B, and F/A. The strands of IgG and D1 are aligned similarly to that presented in a previously published report (Deivanayagam et al., 2000). If any one of the colors on IgG and D1 are aligned, an adjacent strand of D1 (to the right or left) is observed to be on the opposite side in IgG (Deivanayagam et al., 2000). The topology of GBS52 is very similar to that of D1, except that the F strand in GBS52 is shifted to the opposite β sheet, resulting in DAG and CBEF stranded sheets instead of the DAGF and CBE stranded sheets observed in the D1 domain.

atoms. The four- and three-stranded β sheets of GBS52 N1 superimpose with three- and four-stranded β sheets of the IgG constant domain, respectively (Figure 3C). The differences are seen at the loops as well as in the position of the C strand, which is at one end of the three-stranded β sheet and also shows deviation with the D strand that is at another end of the four-stranded β sheet of the IgG constant domain. The N-terminal strand A and the C-terminal strand G of the IgG constant domain superimpose on the C-terminal G and F strands of the GBS52 N1, respectively, and run in opposite directions. Similarly, the superposition of the N2 domain of GBS52 with the IgG domain resulted in an rms deviation of 1.6 Å for 32 common Cα atoms, which indicates that the N2 domain is closer than the N1 to the IgG constant domain.

Topology Comparison of GBS52 N1 and N2 Domains with the Cna B Region Subdomains

Similar topology comparisons between the folds of the collagen-binding surface protein (Cna) B region repeat units (subdomains) and the IgG-like domains (Deivanayagam et al., 2000) revealed an inverse relationship between them (Figures 4A and 4B). The D1 (87 residue) and D2 (97 residue) domains of the Cna B repeat regions are almost identical in superposition, with an rms deviation of 1.28 Å for 87 Cα atoms. These are made of one four-stranded antiparallel β sheet DAGF and another three-stranded antiparallel β sheet EBC (Figure 4B), and their structural fold has been termed as inverse or reverse IgG fold (IgG-rev) (Deivanayagam et al., 2000). It was suggested that, if directionality could be assigned to the folding, the D1 domain (IgG-rev) relied on tail-to-head rather than head-to-tail folding. The inverse nature of this fold is observed in many aspects. For example, the structural superposition of the IgG constant domain (PDB ID code 1DBB) and the D1 domain of the Cna B repeat region revealed the C termini position of the latter to be on the opposite side of the molecule despite the same side start and location for their N termini (Deivanayagam et al., 2000) (Figures 4A and 4B). Similarly, if we view the four-stranded β sheet as the frontal plane of the molecule (Figures 4A and 4B), the CD loop region is on the right side of the IgG whereas it is on the left side in D1.

The N1 and N2 domains of GBS52 display a similar topology seen in the B repeat regions by having one four-stranded antiparallel (CBEF) β sheet on one side and another parallel/antiparallel three-stranded (DAG) β sheet on the opposite side (see Figure 2B). Most importantly, similar dispositions for their N and C termini are seen when compared with the Cna B repeat region subdomains, suggesting an analogous IgG-rev fold for the GBS52 secondary structure (Figure 4C). The automatic superposition of the N1 domain of GBS52 and the D1 domain of the B repeat region coordinates resulted in an rms deviation of 1.5 Å for 48 commons Cα atoms. The AB, BC, and FG loops are longer and DE is shorter than the B repeat D1 domain. Similarly, the superposition of the GBS52 N2 domain with the D1 domain of the B repeat resulted in an rms deviation of 1.2 Å for 48 common Cα atoms, suggesting that the N2 domain is closer than N1 to the D1 domain of the B repeat.

Though the GBS52 fold is similar to the IgG-rev fold seen in the B repeat region, the arrangement of the four- and three-stranded β sheet is slightly different. Strand F, present at the edge of the four-stranded β sheet DAGF in the B repeat region, is switched to the side of the three-stranded β sheet CBE to present GBS52 β sheets with three- and four-stranded arrangement (DAG and CBEF). The automatic structural superposition, using various protein-protein superposition programs based on secondary structural elements for each GBS52 domain with the B repeat subdomains and the IgG constant domains, did not give correct alignments, mainly due to these subtle differences in the arrangement of β strands. The disulfide bridge observed in the IgG fold does not exist in GBS52 nor in the Cna B repeat regions.

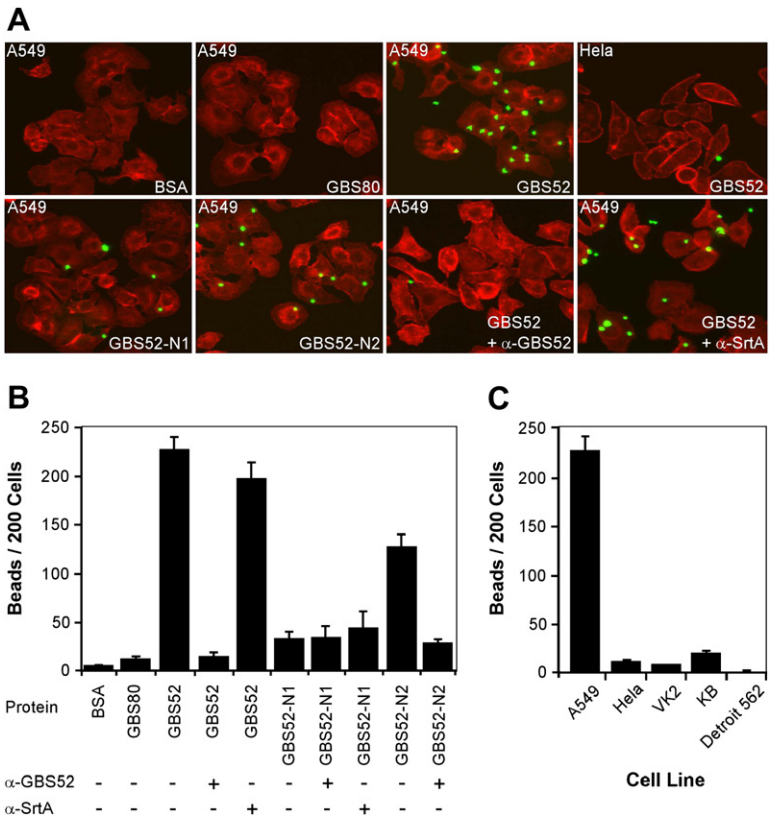

Figure 5. GBS52-Mediated Adherence Specifically to Human Lung Epithelial Cells, A549

(A) Semiconfluent cells grown on coverslips were treated with protein-coated beads. The washed cells were fixed and stained with Texas red-X phalloidin. Shown here are fluorescence images of cells incubated with fluorescent beads bound to BSA, GBS80, GBS52, or GBS52 with HeLa cells, the N1 domain of GBS52, the N2 domain of GBS52, or GBS52 blocked with α-GBS52, or GBS52 blocked with an unrelated antibody against a corynebacterial sortase, α-SrtA.

(B) The results are presented as an average of the number of beads bound per 200 cells of three independent experiments (with standard deviations; ±SD).

(C) Experiments performed as described in (A), except that indicated cells were treated with GBS52 protein-coated beads.

Recombinant GBS52 Protein Binds to Pulmonary Epithelial Cells

The genetic evidence presented above demonstrated that GBS52 acts as an adhesin (Figure 1C). The three-dimensional structure analysis revealed that GBS52 folds into a two-IgG-like domain similar to that found in *Staphylococcus aureus* adhesins (Figure 4). To determine whether the GBS52 pilus protein is sufficient to mediate adherence to host tissues, we expressed different GBS recombinant pilus proteins in *E. coli* and purified these to homogeneity using affinity chromatography (Mandlik et al., 2007). The recombinant proteins were then covalently attached to fluorescent polystyrene beads using primary amine-carboxylate conjugation (see Experimental Procedures). Similar conjugation efficiency by each protein was observed (~30%). An equal amount of beads conjugated to each protein was next added to monolayers of human epithelial cells grown on glass coverslips. After washing, the bound beads were observed by fluorescent microscopy. Adherence was quantified as the average number of beads bound per 200 epithelial cells from three independent experiments.

Remarkably, fluorescent beads coated with the 237 residue GBS52 protein adhered to epithelial cells in an approximately 1:1 ratio, whereas no significant binding was observed for either GBS80- or BSA-coated beads (Figure 5A and first three columns of Figure 5B). This result is in agreement with our observation that GBS80 is not required for bacterial adherence (see Figure 1B). The binding of GBS52-coated beads was inhibited after preincubation with polyclonal antibodies directed against GBS52 (α-GBS52), whereas no significant loss of binding was observed when using antibodies against an irrelevant protein SrtA from *C. diphtheriae* (Figure 5A and fourth and fifth columns of Figure 5B).

To determine whether the N1 and N2 domains of GBS52 are necessary for adhesion to lung epithelial cells, a recombinant protein harboring the N1 or N2 domain was coupled to fluorescent beads as described above. Adherence of N1- or N2-coated beads to A549 cells was then quantified (Figure 5A and last five columns of Figure 5B). Significantly, the isolated N2 domain mediated efficient binding of polystyrene beads to lung cells, a process which was inhibited by antibodies against GBS52. In contrast, the N1-coated beads displayed marginal binding that was unchanged by antibody treatment. The results indicate that the N2 domain of the minor pilin GBS52 contains the binding site for host cell surface receptor and pilin-mediated adherence.

To determine whether the binding of GBS52 to human epithelial cells is specific, we examined the binding of GBS52-coated beads to lung (A549), cervical (HeLa), vaginal (VK2), oral (KB), and pharyngeal (Detroit 562) epithelial cells. GBS52-coated beads adhered avidly to lung epithelial cells but not to others, including both vaginal and cervical epithelial cells (Figure 5C). Taken together, our results demonstrate that GBS52 contains a variant of an IgG-like structure that mediates streptococcal adhesion to the human lung epithelium.

Conclusions

Adherence to specific host tissues is instrumental for many bacterial pathogens to mount successful colonization of humans (Pizarro-Cerda and Cossart, 2006). This host-bacterial interaction is known to be mediated by a variety of cell surface pili (or fimbriae) in the case of several model Gram-negative pathogens (Craig et al., 2003; Freitag et al., 1995; Kikuchi et al., 2005; Kirn et al., 2000; Martinez et al., 2000; Olsen et al., 1989). To date, very little has been reported in this regard for Gram-positive pathogens (see recent review by Telford et al., 2006). In this study, we present the first structural insight, to our knowledge, into how the Gram-positive pilus protein GBS52 mediates bacterial adherence to a specific host tissue. That GBS52 acts as a pilus adhesin was evident from bacterial adherence studies using an ex vivo tissue culture system. Bacterial binding to lung epithelial cells was dramatically reduced (2.5-fold) in a streptococcal mutant that is devoid of *gbs52* as compared to the wild-type strain (Figure 1B). Our crystal structure revealed that a recombinant GBS52 protein of 237 residues forms an extended structure made of two β barrel IgG-rev fold domains N1 and N2 connected by a short linker (Figure 2). The same 237 residue recombinant protein mediates specific binding of latex beads to lung cells, but not to other tested cells of epithelial origin. Most significantly, we show that the N2 domain alone is sufficient for specific host cell binding (Figure 5), revealing that this domain acts as a ligand for specific host cell receptors. A critical next step is to identify this host cell receptor(s) that binds to GBS52.

As *gbs52* is dispensable for the assembly of the streptococcal PI-1-encoded pili (Rosini et al., 2006) and GBS52 does not contain the pilin motif, we hypothesize that the N2 domain of GBS52 pilin may primarily function to mediate specific adherence to pulmonary cells, whereas the N1 domain may perform a structural function. Such a scenario parallels the domain architecture and function of the adhesin present in the P pili of *E. coli* (see Dodson et al., 2001). P pili are composed of repeating PapA subunits forming the pilus rod and the PapG adhesin located at the tip region via the adaptor PapF. Whereas the N terminus of PapG provides the receptor binding domain, its C terminus that harbors the IgG-like fold is involved in a donor strand exchange reaction with PapF, which links PapG to the tip fibrillum. Future experiments should determine whether the N1 domain is required for the incorporation of GBS52 into pilus structures.

It is interesting to note that with only 13% identity between them, the N1 and N2 domains of GBS52 display high structural homology (rms deviation of 1.3 Å for 65 common Cα atoms), possibly suggesting an ancient gene duplication/fusion event. In addition, it has been known (Rich et al., 1998) that the *S. aureus* Cna B repeat region with IgG-rev fold apparently has no adhesive properties, unlike that shown here for GBS52 pilin. Model-building studies, with the help of BLAST, 3D-PSSM, and PHYRE algorithms (http://www.sbg.bio.ic.ac.uk/), using the primary sequences of SpaA-type pili subunits in *C. diphtheriae*, revealed the presence of multiple subdomains having similar IgG-like folds, specifically four of them in SpaA, one in SpaB, and six or more in SpaC (unpublished results). The need to bind and escape the host's hostile innate and adaptive immune responses might have driven the convergent evolution of distinct proteins and their subdomains to a common structure, albeit to perform different functions.

Variants of human immunoglobulin subdomains (IgG) confer adhesive properties to several surface protein MSCRAMMs, such as the collagen-binding protein Cna and the fibrinogen-binding proteins ClfA and ClfB of *S. aureus* (Deivanayagam et al., 2000, 2002; Ponnuraj et al., 2003; Zong et al., 2005). It has been speculated that such mimicry of the host's immune system elements (e.g., immunoglobulin) facilitates, if not the pathogen entry, the definite escape from clearance by the innate immune response such as the complement pathway. It is especially important to point out that the topology of adhesive domains of MSCRAMMs is recognized as variants of the immunoglobulin fold IgG derivative (Deivanayagam et al., 2002; Ponnuraj et al., 2003). The C-terminal protein segments of MSCRAMMs that help the adhesive domain gain access to cellular matrix proteins such as collagen and fibrinogen are recognized to be the unique immunoglobulin reverse fold IgG-rev (Deivanayagam et al., 2000). The latter domains are thought to project the MSCRAMM adhesive domains away from the cell surface and thereby facilitate their escape from the host's extracellular defensive apparatus. In this study, we show that the subdomains of GBS52 display a similar IgG-rev fold and also exhibit an adhesive nature. Whether the presence of such a fold in GBS52 contributes to this defensive mechanism is worthy of future investigation.

EXPERIMENTAL PROCEDURES

Bacterial Strains, Plasmids, and Media

Streptococcus agalactiae 2603V/R was obtained from the American Type Culture Collection (ATCC) (Tettelin et al., 2002). Plasmid pHY304 (Shelver et al., 2003) was generously provided by Craig E. Rubens. GBS strains were grown in Todd Hewitt Broth (THB) supplemented with 0.5% yeast extract and with 1 μg/ml erythromycin as needed. *Escherichia coli* strains were grown in Luria Broth. Erythromycin and ampicillin were added at 300 μg/ml and 100 μg/ml, respectively, as needed. Reagents were purchased from Sigma unless otherwise indicated.

Generation of *S. agalactiae* Deletion Mutants

Nonpolar in-frame deletion mutants of *S. agalactiae* were generated by homologous recombination by a previously described procedure (Cieslewicz et al., 2001). The deletion mutants (see Table S2 in the Supplemental Data available with this article online) were verified by PCR and Southern blotting analysis. Briefly, gene deletions were constructed by crossover PCR using Δ primers (Table S1) and cloned between appropriate restriction sites of the temperature-sensitive *E. coli*/*Streptococcus* shuttle vector pHY304 according to a published procedure (Ton-That and Schneewind, 2003). The generated deletion constructs were introduced into *S. agalactiae* by electroporation, and allelic exchange techniques were performed as previously described (Framson et al., 1997).

Plasmid Construction

Appropriate oligonucleotide primers (H6 primers; Table S1) and *S. agalactiae* 2603V/R chromosomal DNA were used for the PCR amplification of coding sequences for the mature GBS52 (His31–Arg267), the N1 of GBS52 (His31–Ile150), the N2 of GBS52 (Ser152–Arg267), and the mature GBS80 (Arg36–Arg518). Resulting DNA fragments were cloned between appropriate sites of the expression vector pQE30 (QIAGEN) to produce recombinant proteins with an N-terminal hexahistidine tag. The recombinant plasmids were transformed into *E. coli* XL1-Blue. DNA sequencing was done to verify the recombinant plasmids (Table S2).

Purification of Recombinant Proteins

Overnight cultures (40 ml) of stationary-phase *E. coli* were used to inoculate 1 liter of Luria Broth containing 50 μg/ml ampicillin. The cells were allowed to grow at 37°C until the culture reached $OD_{600\ nm}$ ~0.6. Protein expression was induced by addition of isopropyl-β-D-thiogalactopyranoside (IPTG) to a final concentration of 0.2 mM and the culture was incubated overnight at 37°C. After overnight induction, the bacteria were then collected by centrifugation and resuspended in a minimal volume of buffer (20 mM PBS, 150 mM NaCl [pH 7.4]). The cells were lysed by passage through a French press (11,000 psi) twice. Insoluble debris was removed by centrifugation at 20,000 rpm for 20 min at 4°C, and the supernatant was applied to an immobilized metal chelate affinity chromatography column. The column was charged with Ni^{2+}, connected to an FPLC system (Pharmacia). The column was washed with ten bed volumes of 20 mM PBS, 150 mM NaCl (pH 7.4), and bound protein eluted with a linear gradient of 0–250 mM imidazole in 20 mM PBS, 150 mM NaCl (pH 7.4). Fractions containing the desired protein, as determined by SDS-PAGE, were pooled and concentrated using an Amicon ultrafiltration system. The concentrated protein was further applied to an S100 (16/60) Sephacryl gel-filtration column and then concentrated to 20 mg/ml for crystallization experiments.

Crystallization and Data Collection

Crystals of GBS52 (His31–Arg267) with an N-terminal His_6 tag were grown by the hanging-drop vapor-diffusion method. Drops were created using equal volumes (2 μl) of well solution (0.2 M ammonium citrate, 20% PEG1500 in 0.1 M HEPES buffer [pH 7.0], 0.01 M $CaCl_2$) and protein at ~20 mg/ml concentration. Crystals were grown at 4°C and appeared in 2–4 days. Crystals belonged to a monoclinic $P2_1$ space group, with cell dimensions a = 41.5 Å, b = 52.2 Å, c = 61.0 Å, and β = 101.8°, having one molecule in the asymmetric unit. A native diffraction data set was collected on a Rigaku R-axis IV imaging plate detector using CuKα radiation from an in-house Rigaku rotating-anode X-ray generator operating at 100 mA and 50 kV. Eighteen percent ethylene glycol was used as a cryoprotectant and crystals were flash-frozen at 100K using nylon or litho loops. Crystallographic data statistics are presented in Tables 1 and 2.

Structure Determination

The crystal structure was determined by multiple isomorphous replacement methods with the help of three heavy-atom derivatives (2.0 mM $Hg[CH_3COO]_2$, 40 mM K_2PtCl_4, 2 mM $Ag[NO]_3$). All data sets were processed and scaled using the D*TREK program (Pflugrath, 1999) (Table 1). Refinement of heavy-atom derivatives and subsequent phase calculations were carried out with the SOLVE program (Terwilliger and Berendzen, 1999) (Table 2). After several cycles of rebuilding and refinement with the Coot (Emsley and Cowtan, 2004) and CNS (Brunger et al., 1998) programs, 223 water molecules were added in the final cycle's refinement with REFMAC (CCP4, 1994). The final R_{free} and R factor are 23.1% and 19.7, respectively. The refinement statistics are shown in Table 3.

Covalent Coupling of Proteins to Fluorescent Latex Beads

Purified proteins were covalently attached to 1.0 μm carboxylate-modified fluorescent microspheres (Molecular Probes). Covalent protein attachment was performed according to the manufacturer's protocol with modifications. Briefly, ~300 μg of purified protein in 50 mM MES (pH 6.0) and 10^{12} beads were incubated at room temperature for 15 min. The buffer was adjusted to pH 6.5 after the addition of 1.6 mg/ml 1-ethyl-3-(3-dimethylaminopropyl)-carbodiimide hydrochloride (EDAC; Molecular Probes) to activate the surface carboxyl groups and allowed to incubate for 24 hr in the dark with mixing. Glycine was added to a final concentration of 100 mM to quench the reaction. Beads with bound protein were washed and blocked with 2 mg/ml BSA in PBS for 15 hr in the dark at 4°C. The beads were then washed and stored in PBS with 1% BSA in the dark at 4°C. To determine the coupling efficiency, the protein concentration of the supernatant from the first wash (before addition of BSA) was measured using the BCA system (Pierce) and subtracted from the protein concentration in the mixture at the start of the coupling. Similar coupling efficiency (30%) was observed for different recombinant pilus proteins.

Cell Culture

Human cell lines A549 (ATCC CCL-185; alveolar epithelial carcinoma), HeLa (ATCC CCL-2; cervical carcinoma), KB (oral epithelial; a gift from M. Herzberg), VK2 (CRL-2616; vaginal), and Detroit 562 (ATCC CCL-138; pharyngeal carcinoma) were cultured according to ATCC propagation suggestions under 5% CO_2 at 37°C. Twelve-well tissue culture flasks were seeded for 24–48 hr to establish monolayers.

Adhesion Assays

Streptococcal variants were grown to mid-log phase ($OD_{600\ nm}$ ~0.4) in THB from a 1:100 dilution of a stationary overnight culture. Washed bacteria were resuspended to 5×10^7 cfu/ml in RPMI media. Cell monolayers were infected at a multiplicity of infection (MOI) of 10 for 1 hr at 37°C under 5% CO_2. Washed cells were detached with 0.025% trypsin in PBS for 10 min, and lysed by treating with a dilute trypsin-versene mixture (BioWhittaker) and 0.025% Triton X-100. The appropriate dilutions were plated on Todd Hewitt agar plates to enumerate adherent bacteria. The results were obtained from at least three independent experiments performed in quadruplicate.

For immunofluorescence microscopy, human epithelial cells were grown on glass coverslips, blocked with 0.5% BSA in PBS for 30 min at room temperature, and treated with protein-coated beads at an MOI of 100 for 1 hr at room temperature in RPMI. For antibody-blocking experiments, protein-coated beads were incubated with an appropriate antibody (diluted 1:100) for 1 hr at 4°C prior to the treatment of human epithelial cells. Cells with bound beads were washed with PBS, fixed in 3% paraformaldehyde for 10 min at room temperature, and permeabilized with 0.1% Triton X-100 in PBS for 3–5 min. Texas red-X phalloidin (Molecular Probes) was used to stain epithelial cells according to the manufacturer's instructions. The coverslips were mounted and sealed on glass slides.

Microscopy Techniques

Slides were examined by an Olympus BX60 microscope with a 10× objective using Chroma filter sets 41029 for visualizing yellow-green fluorescence (beads) and 31004 for visualizing Texas red (cells). A Hamamatsu Orca digital camera (model C4742-95), Openlab software (Improvision), and Adobe PhotoShop were used to collect and process images.

Supplemental Data

Supplemental Data include two tables and can be found with this article online at http://www.structure.org/cgi/content/full/15/8/893/DC1/.

ACKNOWLEDGMENTS

We thank Craig E. Rubens (University of Washington, Seattle) for providing the pHY304 plasmid, Mark Herzberg (University of Minnesota) for supplies of the KB cell line, and Michael R. Wessels (Harvard Medical School) for reagents. We are grateful to Asis Das, Bing Hao

(University of Connecticut Health Center), and members of our laboratory for valuable discussions and critical review of the manuscript. This work was supported by the Charles H. Hood Foundation and NIH grants AI061381 (to H.T.-T.) and AI064815 (to S.V.L.N.).

Received: February 5, 2007
Revised: June 12, 2007
Accepted: June 15, 2007
Published: August 14, 2007

REFERENCES

Baker, C., and Edward, M. (2001). Group B streptococcal infections. In Infectious Diseases of the Fetus and Newborn Infant, J.S. Remington and J.O. Klein, eds. (Philadelphia: W.B. Saunders), pp. 1091–1156.

Barocchi, M.A., Ries, J., Zogaj, X., Hemsley, C., Albiger, B., Kanth, A., Dahlberg, S., Fernebro, J., Moschioni, M., Masignani, V., et al. (2006). A pneumococcal pilus influences virulence and host inflammatory responses. Proc. Natl. Acad. Sci. USA *103*, 2857–2862.

Brunger, A.T., Adams, P.D., Clore, G.M., DeLano, W.L., Gros, P., Grosse-Kunstleve, R.W., Jiang, J.S., Kuszewski, J., Nilges, M., Pannu, N.S., et al. (1998). Crystallography & NMR System: a new software suite for macromolecular structure determination. Acta Crystallogr. D Biol. Crystallogr. *54*, 905–921.

CCP4 (Collaborative Computational Project, Number 4) (1994). The CCP4 suites: programs for protein crystallography. Acta Crystallogr. D Biol. Crystallogr. *50*, 760–763.

Cieslewicz, M.J., Kasper, D.L., Wang, Y., and Wessels, M.R. (2001). Functional analysis in type Ia group B Streptococcus of a cluster of genes involved in extracellular polysaccharide production by diverse species of streptococci. J. Biol. Chem. *276*, 139–146.

Craig, L., Taylor, R.K., Pique, M.E., Adair, B.D., Arvai, A.S., Singh, M., Lloyd, S.J., Shin, D.S., Getzoff, E.D., Yeager, M., et al. (2003). Type IV pilin structure and assembly: X-ray and EM analyses of *Vibrio cholerae* toxin-coregulated pilus and *Pseudomonas aeruginosa* PAK pilin. Mol. Cell *11*, 1139–1150.

Deivanayagam, C.C., Rich, R.L., Carson, M., Owens, R.T., Danthuluri, S., Bice, T., Hook, M., and Narayana, S.V. (2000). Novel fold and assembly of the repetitive B region of the *Staphylococcus aureus* collagen-binding surface protein. Structure *8*, 67–78.

Deivanayagam, C.C., Wann, E.R., Chen, W., Carson, M., Rajashankar, K.R., Hook, M., and Narayana, S.V. (2002). A novel variant of the immunoglobulin fold in surface adhesins of *Staphylococcus aureus*: crystal structure of the fibrinogen-binding MSCRAMM, clumping factor A. EMBO J. *21*, 6660–6672.

Dietmann, S., Park, J., Notredame, C., Heger, A., Lappe, M., and Holm, L. (2001). A fully automatic evolutionary classification of protein folds: Dali Domain Dictionary version 3. Nucleic Acids Res. *29*, 55–57.

Dodson, K.W., Pinkner, J.S., Rose, T., Magnusson, G., Hultgren, S.J., and Waksman, G. (2001). Structural basis of the interaction of the pyelonephritic *E. coli* adhesin to its human kidney receptor. Cell *105*, 733–743.

Doran, K.S., and Nizet, V. (2004). Molecular pathogenesis of neonatal group B streptococcal infection: no longer in its infancy. Mol. Microbiol. *54*, 23–31.

Dramsi, S., Caliot, E., Bonne, I., Guadagnini, S., Prevost, M.C., Kojadinovic, M., Lalioui, L., Poyart, C., and Trieu-Cuot, P. (2006). Assembly and role of pili in group B streptococci. Mol. Microbiol. *60*, 1401–1413.

Emsley, P., and Cowtan, K. (2004). Coot: model-building tools for molecular graphics. Acta Crystallogr. D Biol. Crystallogr. *60*, 2126–2132.

Fischetti, V.A., Pancholi, V., and Schneewind, O. (1990). Conservation of a hexapeptide sequence in the anchor region of surface proteins from Gram-positive cocci. Mol. Microbiol. *4*, 1603–1605.

Framson, P.E., Nittayajarn, A., Merry, J., Youngman, P., and Rubens, C.E. (1997). New genetic techniques for group B streptococci: high-efficiency transformation, maintenance of temperature-sensitive pWV01 plasmids, and mutagenesis with Tn917. Appl. Environ. Microbiol. *63*, 3539–3547.

Freitag, N.E., Seifert, H.S., and Koomey, M. (1995). Characterization of the pilF-pilD pilus-assembly locus of *Neisseria gonorrhoeae*. Mol. Microbiol. *16*, 575–586.

Gaspar, A.H., and Ton-That, H. (2006). Assembly of distinct pilus structures on the surface of *Corynebacterium diphtheriae*. J. Bacteriol. *188*, 1526–1533.

Gomis-Ruth, F.X., Companys, V., Qian, Y., Fricker, L.D., Vendrell, J., Aviles, F.X., and Coll, M. (1999). Crystal structure of avian carboxypeptidase D domain II: a prototype for the regulatory metallocarboxypeptidase subfamily. EMBO J. *18*, 5817–5826.

Kikuchi, T., Mizunoe, Y., Takade, A., Naito, S., and Yoshida, S. (2005). Curli fibers are required for development of biofilm architecture in *Escherichia coli* K-12 and enhance bacterial adherence to human uroepithelial cells. Microbiol. Immunol. *49*, 875–884.

Kim, J.S., Kluskens, L.D., de Vos, W.M., Huber, R., and van der Oost, J. (2004). Crystal structure of fervidolysin from *Fervidobacterium pennivorans*, a keratinolytic enzyme related to subtilisin. J. Mol. Biol. *335*, 787–797.

Kirn, T.J., Lafferty, M.J., Sandoe, C.M., and Taylor, R.K. (2000). Delineation of pilin domains required for bacterial association into microcolonies and intestinal colonization by *Vibrio cholerae*. Mol. Microbiol. *35*, 896–910.

Mandlik, A., Swierczynski, A., Das, A., and Ton-That, H. (2007). *Corynebacterium diphtheriae* employs specific minor pilins to target human pharyngeal epithelial cells. Mol. Microbiol. *64*, 111–124.

Marraffini, L.A., Dedent, A.C., and Schneewind, O. (2006). Sortases and the art of anchoring proteins to the envelopes of Gram-positive bacteria. Microbiol. Mol. Biol. Rev. *70*, 192–221.

Martinez, J.J., Mulvey, M.A., Schilling, J.D., Pinkner, J.S., and Hultgren, S.J. (2000). Type 1 pilus-mediated bacterial invasion of bladder epithelial cells. EMBO J. *19*, 2803–2812.

Mishra, A., Das, A., Cisar, J.O., and Ton-That, H. (2007). Sortase-catalyzed assembly of distinct heteromeric fimbriae in *Actinomyces naeslundii*. J. Bacteriol. *189*, 3156–3165.

Mora, M., Bensi, G., Capo, S., Falugi, F., Zingaretti, C., Manetti, A.G., Maggi, T., Taddei, A.R., Grandi, G., and Telford, J.L. (2005). Group A Streptococcus produce pilus-like structures containing protective antigens and Lancefield T antigens. Proc. Natl. Acad. Sci. USA *102*, 15641–15646.

Nallapareddy, S.R., Singh, K.V., Sillanpaa, J., Garsin, D.A., Hook, M., Erlandsen, S.L., and Murray, B.E. (2006). Endocarditis and biofilm-associated pili of *Enterococcus faecalis*. J. Clin. Invest. *116*, 2799–2807.

Olsen, A., Jonsson, A., and Normark, S. (1989). Fibronectin binding mediated by a novel class of surface organelles on *Escherichia coli*. Nature *338*, 652–655.

Patti, J.M., Allen, B.L., McGavin, M.J., and Hook, M. (1994). MSCRAMM-mediated adherence of microorganisms to host tissues. Annu. Rev. Microbiol. *48*, 585–617.

Pflugrath, J.W. (1999). The finer things in X-ray diffraction data collection. Acta Crystallogr. D Biol. Crystallogr. *55*, 1718–1725.

Pizarro-Cerda, J., and Cossart, P. (2006). Bacterial adhesion and entry into host cells. Cell *124*, 715–727.

Ponnuraj, K., Bowden, M.G., Davis, S., Gurusiddappa, S., Moore, D., Choe, D., Xu, Y., Hook, M., and Narayana, S.V. (2003). A "dock, lock, and latch" structural model for a staphylococcal adhesin binding to fibrinogen. Cell *115*, 217–228.

Rich, R.L., Demeler, B., Ashby, K., Deivanayagam, C.C., Petrich, J.W., Patti, J.M., Narayana, S.V., and Hook, M. (1998). Domain structure of the *Staphylococcus aureus* collagen adhesin. Biochemistry *37*, 15423–15433.

Rosini, R., Rinaudo, C.D., Soriani, M., Lauer, P., Mora, M., Maione, D., Taddei, A., Santi, I., Ghezzo, C., Brettoni, C., et al. (2006). Identification of novel genomic islands coding for antigenic pilus-like structures in *Streptococcus agalactiae*. Mol. Microbiol. *61*, 126–141.

Scott, J.R., and Zahner, D. (2006). Pili with strong attachments: Gram-positive bacteria do it differently. Mol. Microbiol. *62*, 320–330.

Shelver, D., Rajagopal, L., Harris, T.O., and Rubens, C.E. (2003). MtaR, a regulator of methionine transport, is critical for survival of group B streptococcus in vivo. J. Bacteriol. *185*, 6592–6599.

Spellerberg, B. (2000). Pathogenesis of neonatal *Streptococcus agalactiae* infections. Microbes Infect. *2*, 1733–1742.

Swierczynski, A., and Ton-That, H. (2006). Type III pilus of corynebacteria: pilus length is determined by the level of its major pilin subunit. J. Bacteriol. *188*, 6318–6325.

Symersky, J., Patti, J.M., Carson, M., House-Pompeo, K., Teale, M., Moore, D., Jin, L., Schneider, A., DeLucas, L.J., Hook, M., and Narayana, S.V. (1997). Structure of the collagen-binding domain from a *Staphylococcus aureus* adhesin. Nat. Struct. Biol. *4*, 833–838.

Telford, J.L., Barocchi, M.A., Margarit, I., Rappuoli, R., and Grandi, G. (2006). Pili in Gram-positive pathogens. Nat. Rev. Microbiol. *4*, 509–519.

Terwilliger, T.C., and Berendzen, J. (1999). Automated MAD and MIR structure solution. Acta Crystallogr. D Biol. Crystallogr. *55*, 849–861.

Tettelin, H., Masignani, V., Cieslewicz, M.J., Eisen, J.A., Peterson, S., Wessels, M.R., Paulsen, I.T., Nelson, K.E., Margarit, I., Read, T.D., et al. (2002). Complete genome sequence and comparative genomic analysis of an emerging human pathogen, serotype V *Streptococcus agalactiae*. Proc. Natl. Acad. Sci. USA *99*, 12391–12396.

Ton-That, H., and Schneewind, O. (2003). Assembly of pili on the surface of *Corynebacterium diphtheriae*. Mol. Microbiol. *50*, 1429–1438.

Ton-That, H., and Schneewind, O. (2004). Assembly of pili in Gram-positive bacteria. Trends Microbiol. *12*, 228–234.

Ton-That, H., Marraffini, L.A., and Schneewind, O. (2004). Sortases and pilin elements involved in pilus assembly of *Corynebacterium diphtheriae*. Mol. Microbiol. *53*, 251–261.

Zong, Y., Xu, Y., Liang, X., Keene, D.R., Hook, A., Gurusiddappa, S., Hook, M., and Narayana, S.V. (2005). A 'Collagen Hug' model for *Staphylococcus aureus* CNA binding to collagen. EMBO J. *24*, 4224–4236.

Accession Numbers

The coordinates of GBS52 have been deposited in the Protein Data Bank under ID code 2PZ4.